The Journal of Veterinary Medical Science

FULL PAPER

Anatomy

The unique physiological features of the broiler pectoralis major muscle as suggested by the three-dimensional ultrastructural study of mitochondria in type IIb muscle fibers

Marina HOSOTANI[1)], Kiyokazu KAMETANI[1)], Nobuhiko OHNO[2,3)], Kohzy HIRAMATSU[4)], Takeshi KAWASAKI[5)], Yasuhiro HASEGAWA[6)], Tomohito IWASAKI[6)]* and Takafumi WATANABE[1)]*

[1)]Department of Veterinary Anatomy, School of Veterinary Medicine, Rakuno Gakuen University, Ebetsu, Hokkaido 069-8501, Japan
[2)]Division of Ultrastructural Research, National Institute for Physiological Science, Okazaki, Aichi 444-8585, Japan
[3)]Division of Histology and Cell Biology, Department of Anatomy, Jichi Medical University, Shimotsuke, Tochigi 329-0498, Japan
[4)]Laboratory of Animal Functional Anatomy (LAFA), Faculty of Agriculture, Shinshu University, Kami-ina, Nagano 399-4598, Japan
[5)]Research Office Concerning the Health of Humans and Birds, Abashiri, Hokkaido 099-3119, Japan
[6)]Department of Food Science and Human Wellness, College of Agriculture, Food and Environment Science, Rakuno Gakuen University, Ebetsu, Hokkaido 069-8501, Japan

ABSTRACT. Typical skeletal muscles are composed of mixed muscle fiber types, which are classified as slow-twitch (type I) and fast-twitch (type II) fibers, whereas pectoralis major muscles (PMs) in broiler chickens are 100% composed of type IIb fast-twitch fibers. Since metabolic properties differ among muscle fiber types, the combination of muscle fiber types is involved in physiological functions and pathological conditions in skeletal muscles. In this study, using serial block-face scanning electron microscopy, we compared three-dimensional (3D) mitochondrial properties in type IIb fibers in broiler PMs and those in type I fibers of broiler gastrocnemius muscles (GMs) heterogeneously composed of slow- and fast-twitch muscle fibers. In type I fibers in the GMs, elongated mitochondria with numerous interconnections to form a substantial network among myofibrils were observed. Along with lipid droplets sandwiched by mitochondria, these features are an adaptation to effective oxidative respiration and constant oxidative damage in slow-twitch muscle fibers. In contrast, type IIb fibers in the PMs showed small and ellipsoid-shaped mitochondria with few interconnections and no lipid droplets, forming a sparse network. The mitochondrial spatial network comprises of active mitochondrial dynamics to reduce mitochondrial damage; therefore, type IIb fibers possess physiologically low capacity to maintain mitochondrial wellness due to static mitochondrial dynamics. Based on 3D mitochondrial properties, we discussed the contrasting physiological functions between type I and IIb fibers and proposed a high contractile power and low stress resistance as unique physiological properties of broiler PMs.

KEY WORDS: 3D reconstruction, mitochondria, slow-/fast-twitch muscle, ultrastructure, wooden breast syndrome

J. Vet. Med. Sci.
83(11): 1764–1771, 2021
doi: 10.1292/jvms.21-0408

Received: 21 July 2021
Accepted: 5 September 2021
Advanced Epub:
15 September 2021

Skeletal muscle fibers in vertebrates are heterogeneously composed of two types of muscle fibers: slow-twitch (type I) and fast-twitch (type II), which are classified based on their contractility, electrophysiological features, and differences in energy production [21]. Fast-twitch muscle fibers are classified further into three subtypes—IIa, IIx, and IIb—according to the differences in the gene expression of the myosin heavy chain [21]. Variations in the compositions of muscle fiber types yield susceptibility differences against both hereditary and acquired skeletal muscle disorders [21].

*Correspondence to: Iwasaki, T.: iwasaki@rakuno.ac.jp, Watanabe, T.: t-watanabe@rakuno.ac.jp
(Supplementary material: refer to PMC https://www.ncbi.nlm.nih.gov/pmc/journals/2350/)

In broiler chickens, pectoralis major muscles (PMs) are 100% composed of type IIb fibers, whereas a mixture of different muscle fiber types comprises broiler systemic skeletal muscles other than the PMs [8, 17]. Curiously, severe myopathy such as wooden breast syndrome (WB) is specific to the PMs in the systemic skeletal muscles [18]. The WB pathologies, including hemorrhages, pale color, and hardness, are triggered by hypoxia stress resulting from insufficient blood supply against rapid PM growth [16, 20]. Along with the genetic background of the broilers exhibiting the phenotype of significant PM growth [1], the unique composition of muscle fiber types and physiological features in the PMs is considered to be a factor in the specificity of WB expression in PMs.

Focusing on the distinct energy production among muscle fiber types, type I and IIa fibers produce adenosine triphosphate (ATP) dependent on oxidative phosphorylation, while IIx and IIb fibers undergo glycolytic metabolism to produce energy [12]. This metabolic difference corresponds to the mitochondrial differences in quantity and quality among muscle fiber types [6]. In recent years, the three-dimensional (3D) ultrafine investigation methods of organelle structure have revealed differences in mitochondrial 3D morphologies, distributions, and networks in mammalian skeletal muscle fibers [7, 27]. Mitochondria dynamically and kinetically transform their morphology by fusion and fission in response to various physiological and pathological cellular statuses [13]. A mitochondrial spatial network is then built through the interaction of the mitochondrial liner complex or scattered individual mitochondria [31]. Mitochondrial dynamics and interactions are essential for skeletal muscle homeostasis by the clearance of damaged mitochondria; that is, the dysfunction and destruction of the mitochondrial dynamics and network cause myopathy [19, 27]. Mitochondrial membrane projections connecting two non-adjacent mitochondria are more frequently observed in the skeletal muscle of human patients with genetic defects in mitochondrial function than in healthy humans. This is considered a compensatory hyperfusion against mitochondrial stress [27]. In obese mice, decreased mitochondrial fusion and increased fission lead to disturbed mitochondrial respiratory function in the skeletal muscle [15]. In broilers, reduced mitochondrial dynamics in PMs are closely related to WB deterioration [9]. Therefore, mitochondrial spatial properties seem to be a good evidence for discussing mammalian and WB myopathies.

The physiological and fundamental information in 3D observations of the mitochondria of broiler skeletal muscles is essential because the 3D mitochondrial structures show species-dependent differences [27]; however, the mitochondrial spatial network has not yet been visualized in broiler PMs. Furthermore, there are no reports that analyzed 3D mitochondrial structure with a distinction among specific muscle fiber subtypes in vertebrates and discussed its relation with the physiological function. Therefore, we determined the 3D mitochondrial morphology, distribution, and network in type IIb fibers in the PMs and type I fibers in the gastrocnemius muscles (GMs) of broilers, which show the most contrasting physiological functions.

MATERIALS AND METHODS

Animals and Specimens

The animal experiments were approved by the Institutional Animal Care and Use Committee of Rakuno Gakuen University (No. DH16A2), in accordance with the Act on Welfare and Management of Animals of the Japanese government. Four broiler chickens (ROSS 308) at 55 days of age raised in the university farm were euthanized by exsanguination under deep anesthesia by intraperitoneal injection of 20–30 mg/kg pentobarbital sodium (Somnopentyl; Kyoritsu Pharmaceutical Co., Tokyo, Japan). The left PMs and GMs were collected, immediately cut into small pieces using razor blades, and immersed in fixative solutions. Four broilers were determined to be unaffected by WB through breast palpitation and wing lift examination by gently lifting the wings to assess the ability to back-to-back wing contact [11]. In addition, histology of PMs was used as an evidence of unaffected muscle fibers without severe myopathy (Supplementary Fig. 1) [9].

Double-immunofluorescence staining for myosin heavy chain in slow-switch muscle fibers and mitochondria

The muscle samples were fixed with Bouin's fixative (Polysciences Inc., Warrington, PA, USA) at 4°C overnight and embedded in paraffin wax according to standard procedures. The paraffin sections were cut into 5-µm-thick sections and mounted on silane-coated glass slides. All washing, blocking, and primary/secondary antibody reactions were performed using a commercial kit (Opal Multiplex IHC Kit; Perkin Elmer Co., Waltham, MA, USA) according to the manufacturer's instructions. Briefly, the sections were incubated overnight at room temperature with the primary antibody, mouse anti-myosin heavy chain of slow-twitch (type I) muscle fibers (MHCI, M8421; Sigma Aldrich Co., LLC, St. Louis, MO, USA) diluted 1:10,000 with immune reaction enhancer solution (Can Get Signal; Toyobo Co., Ltd., Osaka, Japan) to detect type I fibers. After three washes in tris-buffered saline with Tween 20 (TBST), the sections were incubated with polymer horseradish peroxide (HRP)-conjugated secondary antibody for 10 min at room temperature, and the immune complex was visualized with a fluorophore solution (Opal 520 Fluorophore) for 10 min at room temperature. The glass slides were treated with microwaves to strip the primary-secondary-HRP complex and allow the introduction of another mouse primary antibody. After three washes with 0.01 M phosphate-buffered saline (PBS), the sections were incubated with blocking reagent (Blocking One Histo; Nacalai Tesque Co., Kyoto, Japan) for 10 min at room temperature and then with mouse anti-β subunit of ATP synthase (ATPB) antibody (3D5; Abcam Co., Cambridge, UK) diluted 1:500 with Can Get Signal overnight at room temperature to detect the mitochondria. The sections were incubated with CF 568-conjugated goat anti-mouse immunoglobulin G (IgG) antibody diluted 1:300 in PBS for 10 min at room temperature. After three washes with PBS, the sections were mounted with 4′,6-diamidino-2-phenylindole (DAPI) mounting reagent (Nacalai Tesque Co.) and coverslips and were observed using a confocal laser scanning microscope (FV1000D-IX81; Olympus, Tokyo, Japan) equipped with selective Alexa 405, Alexa 488, and Alexa 568 filters. Images were obtained using Fluroview software (Olympus).

Transmission electron microscopy

Muscle samples for transmission electron microscopy were fixed with half-Karnovsky's fixative (2% paraformaldehyde + 2.5% glutaraldehyde in 0.1 M cacodylate buffer, pH 7.4) at 4°C overnight. The contrast of the tissue membrane structure in electron microscopy was enhanced by heavy metal block staining, as described previously [24]. Briefly, the samples were immersed in 1.5% potassium ferrocyanide + 2% osmium tetroxide for 1 hr at 4°C, followed by infiltration with 1% thiocarbohydrazide for 20 min at room temperature, then 2% osmium tetroxide for 30 min at room temperature, and finally in filtered 1% uranyl acetate at 4°C overnight. The samples were then immersed in Walton's lead aspartate solution for 30 min at 60°C and dehydrated with an ethanol series, transferred into QY-1, and finally embedded in epoxy resin (Quetol 812; Nissin EM Co., Ltd., Tokyo, Japan). After polymerization, the tissue blocks were sliced into 80-nm-thick sections perpendicular to the long axis of the muscle fibers using an ultramicrotome (Super Nova; Reichert-Jung, Burladingen, Germany). The sections were collected on a 200-mesh copper grid for 2D observations using a transmission electron microscope (JEM-1400; JEOL Ltd., Tokyo, Japan) at an acceleration voltage of 80 kV. Five muscle fibers were selected from each of the four specimens and observed at × 1,000 (n=20 per slow- or fast-twitch muscle fiber). The obtained images were trimmed to 6,400 (80 × 80) nm^2 squares. The percentage of mitochondrial area in muscle fibers and the area of a mitochondrion from each cropped image was measured using image analysis software (Image J; National Institutes of Health, Bethesda, MD, USA).

Serial block-face scanning electron microscopy

The ultra-thin sliced blocks were trimmed to approximately 0.5 × 0.5 × 1 mm and mounted on an aluminum rivet with conductive adhesive. To avoid charging, the samples were sputtered with gold to increase their conductivity and placed in a scanning electron microscope (SEM) (Merlin or Sigma; Carl Zeiss Inc., Oberkochen, Germany) equipped with a Gatan 3view system for serial block-face SEM, which allows the acquisition of serial images in the z-direction with sectioning and imaging of samples. At least 1,000 serial images (5.0 or 6.0 nm/pixel, 50-nm interval) were collected from each PM and GM.

3D reconstruction

Two hundred serial images were selected from all serial images, yielding 3D images with a depth of 10 µm. The 3D images were produced from the selected serial images using image analysis software (Image-Pro 3D module version 10.0.4; Nippon Roper Co., Tokyo, Japan). The mitochondrial outer membranes were manually traced to reconstruct the 3D structures of individual mitochondria and their networks. The mitochondrion surrounded by a continuous membrane was determined to be one mitochondrion. The 3D reconstruction was automatically performed by Image-Pro 3D module system based on manually traced structures. In addition, 3D images of lipid droplets were constructed. The mitochondrial volume (μm^3) of each reconstructed mitochondrion was automatically calculated using the Image-Pro 3D module system. The mitochondrial volume in muscle fibers was calculated as follows: Mitochondrial volume in muscle fibers (%)=100 × sum of each mitochondrial volume (μm^3) in observed muscle fibers/volume of observed muscle fibers (μm^3). The volume of the observed muscle fibers (μm^3) was calculated as the unit volume of a cube composed of muscle fibers with dimensions 8 × 8 × 10 µm per side. Some planes were selected in the reconstructed figures for specific observations of the mitochondrial interconnection and sarcomere Z-lines (Figs. 3 and 4).

Statistical analysis

The results are expressed as mean ± standard error (SE). Data between two groups were compared using Student's *t*-tests ($P<0.05$), while data among three or more groups are presented in Supplementary Tables 1 and 2 were compared using Tukey's test ($P<0.05$).

RESULTS

Identification of type I fibers in the GMs

Type I fibers were shown as MHCI-positive reaction and randomly observed in broiler GMs (Fig. 1a), revealing that broiler GMs are heterogeneously composed of both slow- and fast-twitch muscle fibers. Previous reports have shown greatly higher mitochondrial density in slow-twitch muscle fibers than in fast-twitch muscle fibers [22]. In broiler GMs, MHCI-positive type I slow-twitch muscle fibers highly co-expressed ATPB (as a marker for mitochondria), whereas MHCI-negative fast-twitch muscle fibers did not (Fig. 1a–d). Type I slow-twitch muscle fibers contain obviously higher numbers of mitochondria than fast-twitch muscle fibers in broiler GMs. Therefore, type I fibers were identified for the following ultrastructural observations based on the index of a high dense population of mitochondria in muscle fibers.

2D observations of mitochondria by transmission electron microscopy

As the PMs in broiler chickens are 100% composed of type IIb fibers [8], all observed muscle fibers in the PMs are classified as type IIb fibers. The type IIb fibers of the PMs showed small mitochondria scattered among myofibrils (Fig. 2a). In contrast, type I fibers of the GMs showed large mitochondria densely distributed among myofibrils (Fig. 2b), corresponded to the immunofluorescence observations (Fig. 1). Numerous lipid droplets adhered to mitochondria, some of which appeared to be included in the intra-membrane of mitochondria (Fig. 2b). The statistical analysis showed that both the percentage of mitochondrial area in muscle fibers and the mitochondrion area were significantly higher in type I fibers than in type IIb fibers (Table 1). Although the mitochondrion areas in both type I and IIb fibers showed individual differences, the percentage of mitochondrial area in muscle fibers in both type I and IIb fibers did not show individual differences (Supplementary Tables 1 and 2). The 3D reconstructions were performed for one of the four PM and GM specimens.

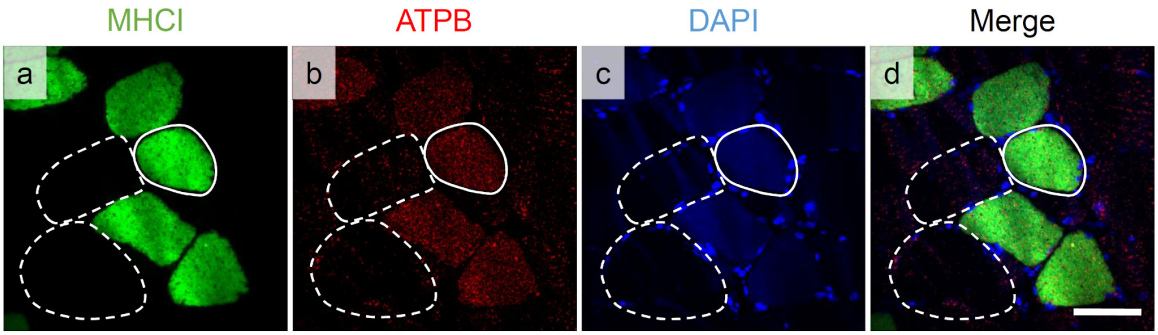

Fig. 1. Immunofluorescence analysis of the gastrocnemius muscle revealing protein expression of slow-twitch (type I) muscle fiber (MHCI; **a**) and mitochondria-specific enzyme (ATPB; **b**). The type I muscle fibers highly co-expressing MHCI and ATPB are surrounded by white lines, while fast-twitch muscle fibers scarcely expressing MHCI nor ATPB are surrounded by white dashed lines in **a**–**d**. Bar=50 µm. MHCI: myosin heavy chain of slow-twitch (type I) muscle fibers, ATPB: β subunit of ATP synthase.

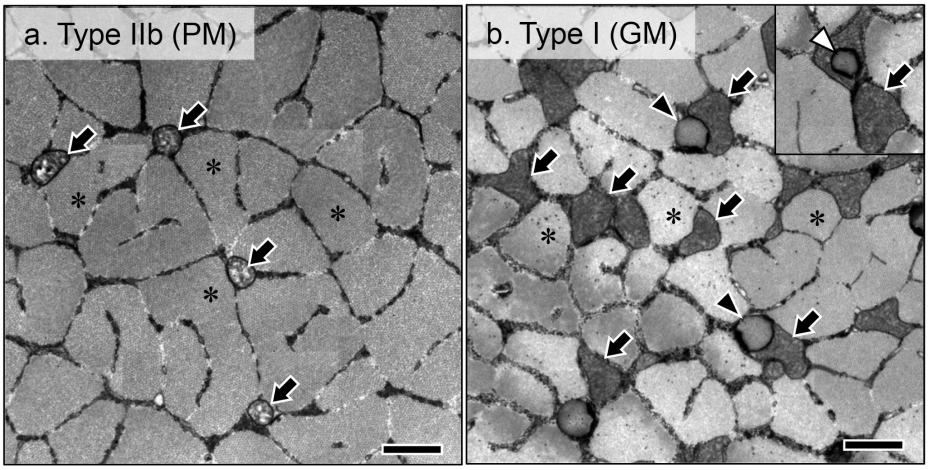

Fig. 2. Two-dimensional ultrastructure of mitochondria in type IIb muscle fibers in the pectoralis major muscle (PM; **a**) and in type I muscle fibers in the gastrocnemius muscle (GM; **b**) revealed by transmission electron microscopy. Bars=1 µm. Arrows: mitochondria among myofibrils, Black arrowheads: lipid droplets adhered to mitochondria, White arrowhead: lipid droplet including the intra-membrane of mitochondria, asterisks: myofibrils.

3D observations of mitochondria by serial scanning electron microscopy

The mitochondria in type IIb fibers showed small size and ellipsoid shape and were sparsely distributed among myofibrils (Fig. 3a and Supplementary Movie 1). The individual mitochondria showed few interconnections and fragmented networks: a few mitochondria possessed nanotunnels (as indicated by arrowheads in Fig. 3b–b" and 3c–c"); that is, the thin membranous interconnection between mitochondria [27], but most were simply located near each other (as indicated by arrows in Fig. 3b–b" and 3c–c"). In contrast, the mitochondria in type I fibers were elongated parallel to the myofibril arrangement and each mitochondrion was interconnected to build a large column structure among myofibrils (Fig. 4a and Supplementary Movie 2). The substantial structures were connected via numerous nanotunnels located along the sarcomere Z-lines to form a more extensive network among myofibrils than that in type IIb fibers (Fig. 4b–b"). In addition, lipid droplets were distributed regularly in the sarcomere Z-lines and were embraced by a mitochondrion or sandwiched between mitochondria (Fig. 4c–c"' and 4d–d"). The percentage of mitochondrial volume in the volume of muscle fibers and the mitochondrion volume are shown in Table 2. Both indices were significantly larger in type I fibers than in type IIb fibers.

Table 1. The mitochondrial area in muscle fibers and the area of a mitochondrion observed in transmission electron microscopy

	Mitochondrial area in the muscle fibers (%)	Mitochondrion area (μm^2)
Type I	8.67 ± 1.53*	0.35 ± 0.087*
Type IIb	1.33 ± 0.48	0.15 ± 0.062

*Significant differences between type I and IIb muscle fibers ($P<0.05$, Student's *t*-test).

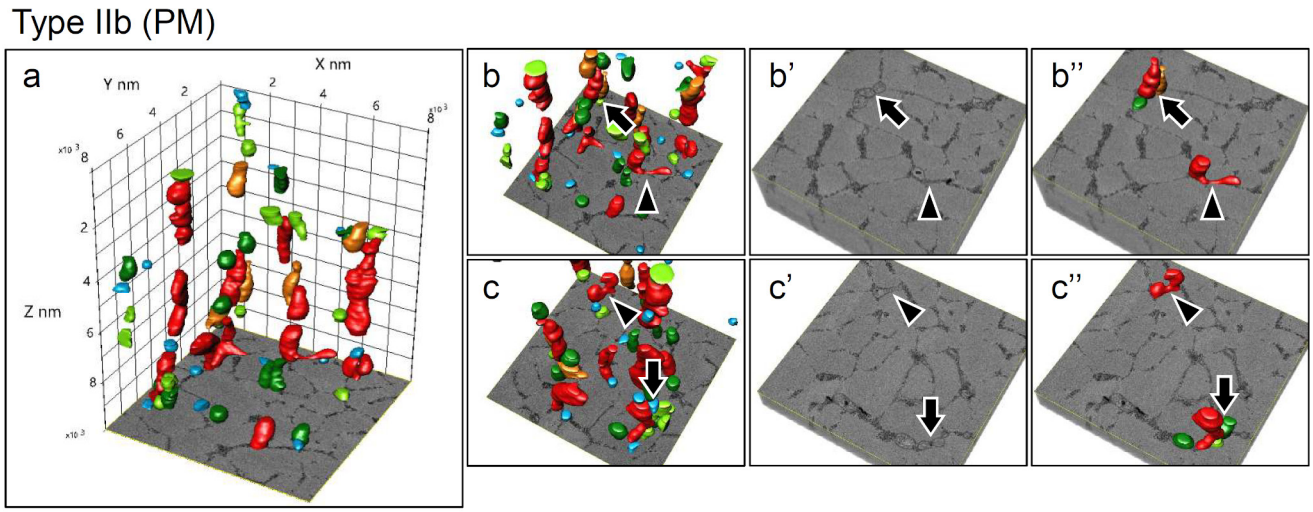

Fig. 3. Three-dimensional ultrastructure of mitochondria in type IIb muscle fibers in the pectoralis major muscle (PM) revealed by serial block-face scanning electron microscopy. **a:** Macro-perspective fragmented mitochondrial spatial network among myofibrils. The colors represent mitochondrial volume (light blue: <0.05 μm^3, light green: 0.05–0.1 μm^3, green: 0.1–0.2 μm^3, orange: 0.2–0.25 μm^3, red: 0.25–1.5 μm^3). **b** and **c** represent views of image **a** observed from different angles. **b'/b"** and **c'/c"** represent the electron microscopy images at the plane including arrows and arrowheads in **b** and **c**, respectively, which display individual mitochondrial connections and positional relationship. Arrows: mitochondria without interconnections, arrowheads: nanotunnels connecting mitochondria.

Table 2. The mitochondrial volume in muscle fibers and the volume of a mitochondrion observed in three-dimensional reconstructed muscle fibers

	Mitochondrial volume in the muscle fibers (%)	Mitochondrial volume (μm^3)
Type I	10.71 ± 0.35*	0.96 ± 0.097*
Type IIb	1.59 ± 0.15	0.15 ± 0.016

*Significant differences between type I and IIb muscle fibers (P<0.05, Student's t-test).

DISCUSSION

Both the 2D and 3D ultrastructural observations of broiler muscle fibers showed a higher content of mitochondria and lipid droplets in type I fibers compared to type IIb fibers. However, the 2D mitochondrial observations could not show the substantial mitochondrial size, shape, and network frame among the myofibrils. Since mitochondria are continuously changing shape [25], mitochondrial appearances in the sectional plane are insufficient evidence to investigate mitochondrial interactions in the muscle. In this study, absolute indices of the plane area of a mitochondrion in muscle fibers showed individual variations among the four observed specimens (Supplementary Tables 1 and 2). Moreover, although the lipid droplets appeared to be located in the mitochondria in the 2D observations, the 3D observations revealed that they were instead embraced by the complex shape of mitochondria and located outside the mitochondrial membrane. Thus, as discussed in mammalian studies [4, 7, 27], 3D mitochondrial observation is the most effective method of investigating mitochondrial spatial properties in the organs.

This study is the first to report a 3D mitochondrial spatial network specific to type IIb muscle fibers in vertebrates. Muscle fiber subtypes (i.e., type I and IIb) have not been clearly distinguished in previous observations of murine or human 3D mitochondrial morphological examinations of the tibialis anterior, soleus, or vastus lateralis muscles because these muscles consist of heterogeneous types of muscle fibers. Moreover, humans do not possess type IIb myosin chain [4, 7, 27]. Previous studies on human muscles using confocal microscopy have reported that the mitochondrial volume in type I and II fibers was 11.9% and 8.6%, respectively, that type I fibers have tubular, highly interconnected mitochondrial spatial networks and that type II fibers possess thinner and shorter tubular interconnections [7]. In contrast, we revealed that the mitochondrial volume in type I and IIb fibers was 10.7% and 1.6%, respectively and that the broiler IIb fibers show fragmented mitochondria with few interconnections. Type II fibers are classified into fast-twitch muscle fibers; however, type II fiber subtypes (i.e., IIa, IIb, and IIx fibers) exhibit differences in metabolic type or biological properties [21]. Type IIa fibers mainly use oxidative metabolism; therefore, they are considered to be the intermediate type between type I and IIx fibers. Type IIx fibers rely on glycolytic metabolism, similar to type IIb fibers; they are intermediate type between type IIa and IIb fibers, showing more fatigue resistance and slower contraction speed than type IIb fibers [14]. Taking into account the differences in the physiological features of type II fibers, the mitochondrial

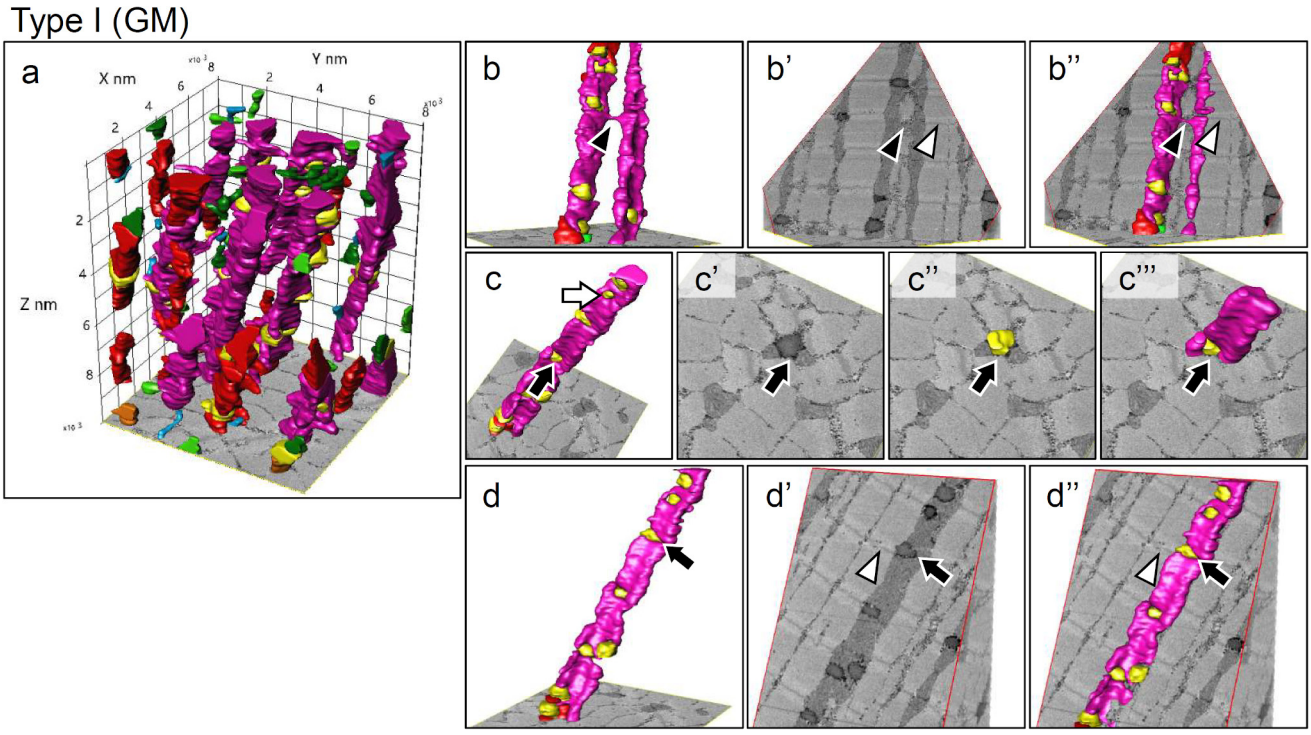

Fig. 4. Three-dimensional ultrastructure of mitochondria in type I muscle fibers in the gastrocnemius muscle (GM) revealed by serial block-face scanning electron microscopy. **a:** Macro perspective of the highly interconnected mitochondrial spatial network among myofibrils. The colors represent mitochondrial volume (light blue: <0.05 μm^3, light green: 0.05–0.1 μm^3, green: 0.1–0.2 μm^3, orange: 0.2–0.25 μm^3, red: 0.25–1.5 μm^3, pink: >1.5 μm^3). Yellow indicates lipid droplets. **c** and **d** represent views of the characteristic mitochondria in image **a** observed from different angles. **b'/b", c'–c"',** and **d'/d"** represent the electron microscopy images at the plane including black arrows and black arrowheads in **b**, **c**, and **d**, respectively. **b–b"** represent mitochondrial column structures connected by nanotunnel located along the sarcomere Z-lines. **c–c"'** represent lipid droplets embraced by a mitochondrion and sandwiched by mitochondria. **d–d"** represent lipid droplets embraced by a mitochondrion located along the sarcomere Z-lines. Black arrowheads: nanotunnels connecting mitochondria, white arrowheads: the sarcomere Z-lines, white arrow: lipid droplets embraced by a mitochondrion, black arrows: lipid droplets sandwiched by mitochondria.

occupancy in type IIb fibers is thought to be the lowest among type II fiber subtypes. Further investigations are needed to determine whether the 3D mitochondrial morphology observed in type IIb fibers in broiler PMs is a universal feature in broiler systemic skeletal muscle and is common among animal species.

The mitochondrial spatial property corresponds to a physiological phenotype specific to muscle fiber types. It has been considered that mitochondrial content is correlated with oxidative capacity, fiber contractile power, and mitochondrial interconnection with metabolic activity status [4, 29]. When discussing these correlations in the broiler muscle, high mitochondrial density represents a high demand for ATP through oxidative phosphorylation in type I fibers; conversely, low mitochondrial density represents a low demand for oxidative energy in type IIb fibers [4, 7]. In contrast, the fewer muscle fibrils relative to the space at the expense of high mitochondrial content weaken the contraction of type I fibers; conversely, more fibrils strengthen the contraction of type IIb fibers. Moreover, the highly interconnected mitochondria that build the column structure undergo active respiratory metabolism in type I fibers while fragmented mitochondria with scarce interconnections perform static and inactive respiratory metabolism in type IIb fibers [29]. Lipid droplets that physically interact with the mitochondria (i.e., peridroplet mitochondria) observed in human type I fibers contribute to the efficient delivery of fatty acids for oxidative energy production, reduction of the potential lipotoxicity, and maintenance of organelle homeostasis under damage [3, 10, 23]. As for broilers, compared to type I fibers with numerous peridroplet mitochondria, the scarcity of peridroplet mitochondria indicates lower endurance for the energy supply and lower resistance to cellular stress in type IIb fibers. In addition, the Z-line width is reportedly thinner in type II fibers than in type I fibers [18]; thus, Z-lines in type IIb fibers in the PMs were unclear in the present study. Generally, skeletal muscles exhibit a hybrid composition of fast- and slow-twitch fibers (i.e., I/IIa, IIa/IIx, and IIx/IIb), which adjusts the balance between muscle power, energy homeostasis, and stress resistance [21]. On the other hand, it is assumed that the broiler PMs composed entirely of type IIb fibers have the fastest and strongest contraction power among systemic skeletal muscles due to their almost exclusive glycolytic energy production at the cost of mitochondrial activity and stress resistance.

The column mitochondrial aggregate and its network spread among the myofibrils are formed by the active remodeling of mitochondrial membranes through fusion and fission (i.e. mitochondrial dynamics) [19], which is the adaptation to metabolic demand relied on oxidative phosphorylation in a muscle cell. Mitochondria are constantly exposed to highly reactive superoxide

produced as a byproduct of oxidative energy production [30]. Active mitochondrial dynamics also play roles in the elimination of oxidative damage to the mitochondria: fusion dilutes the damage to healthy mitochondria [5] while fission segregates damage in one mitochondrion, which is removed by mitophagy [2]. Nanotunnels are double-membrane tubular projections of mitochondria with a diameter of 40–200 nm and a length of 30 µm, which connect non-adjacent mitochondria. They are capable of transporting proteins among connected mitochondria [26, 27] and are presumed to be hyperfusions acting as an initial stress response [27]. Therefore, broiler oxidative type I fibers with a substantial mitochondrial network may have a physiologically high capacity to maintain mitochondrial wellness via active mitochondrial dynamics. In contrast, glycolytic type IIb fibers in broilers with a poor mitochondrial spatial network may not have sufficient adaptability to cellular stress. Broiler PMs exhibit WB, namely severe myopathy, including vacuolization, hypertrophy, and degeneration of myofibers, under chronic and excessive hypoxia [9]. The lower physiological adaptability to oxidative stress in type IIb fibers comprising the PMs might be involved in WB pathogenesis. Further investigation is required to clarify whether oxidative stress in muscle cells can induce active mitochondrial dynamics in type IIb fibers.

The differences in muscle fiber types would reflect the differences in susceptibility to the myopathy. For instance, contrary to oxidative fibers vulnerable to disuse-related muscle atrophy, glycolytic fibers are vulnerable to nutrient-related muscle atrophy [28]. Autophagy inhibition and enzymatic dysfunction specific to glycolytic fibers may explain why certain myopathies target particular muscle fiber types [21, 28], although the entire scope largely remains unsolved. The broiler systemic skeletal muscles, except for the PMs, yield a continuous range of adaptability to oxidative stress owing to the varying composition of oxidative (type I or IIa) and glycolytic (type IIb) fibers in the muscle group that may allow them to avoid the expression of severe myopathies even when exposed to hypoxia. Therefore, the mitochondrial physiological phenotype in type IIb fibers of broilers may explain why WB expression is restricted to PMs. In addition, future investigations of 3D mitochondrial properties of PMs exhibiting severe WB should provide valuable evidence for the involvement of abnormal mitochondrial dynamics in WB pathogenesis.

In conclusion, based on the mitochondrial spatial properties of type IIb fibers, we propose a high contractile power and low stress resistance as unique physiological properties of broiler PMs. This physiological information contributes to an understanding of differences in mitochondrial 3D features among muscle fiber types and could serve as the basis for future investigations of WB pathogenesis.

CONFLICTS OF INTEREST. The authors declare no conflicts of interest.

ACKNOWLEDGMENTS. The authors thank Atsuko Imai and Sei Saitoh (National Institute for Physiological Science) for technical support. This work was supported by Grant-in-Aid Scientific Research (C) from the Japan Society for the Promotion of Science (No. 18K05941 to T.W. and No. 17K08067 to T.I.), and Rakuno Gakuen University Research Fund (No. 2021-04 to T.W.). This study was supported by the Cooperative Study Program of the National Institute for Physiological Sciences.

REFERENCES

1. Bailey, R. A., Watson, K. A., Bilgili, S. F. and Avendano, S. 2015. The genetic basis of pectoralis major myopathies in modern broiler chicken lines. *Poult. Sci.* **94**: 2870–2879. [Medline] [CrossRef]
2. Balog, J., Mehta, S. L. and Vemuganti, R. 2016. Mitochondrial fission and fusion in secondary brain damage after CNS insults. *J. Cereb. Blood Flow Metab.* **36**: 2022–2033. [Medline] [CrossRef]
3. Benador, I. Y., Veliova, M., Mahdaviani, K., Petcherski, A., Wikstrom, J. D., Assali, E. A., Acín-Pérez, R., Shum, M., Oliveira, M. F., Cinti, S., Sztalryd, C., Barshop, W. D., Wohlschlegel, J. A., Corkey, B. E., Liesa, M. and Shirihai, O. S. 2018. Mitochondria bound to lipid droplets have unique bioenergetics, composition, and dynamics that support lipid droplet expansion. *Cell Metab.* **27**: 869–885.e6. [Medline] [CrossRef]
4. Bleck, C. K. E., Kim, Y., Willingham, T. B. and Glancy, B. 2018. Subcellular connectomic analyses of energy networks in striated muscle. *Nat. Commun.* **9**: 5111. [Medline] [CrossRef]
5. Byrne, J. J., Soh, M. S., Chandhok, G., Vijayaraghavan, T., Teoh, J. S., Crawford, S., Cobham, A. E., Yapa, N. M. B., Mirth, C. K. and Neumann, B. 2019. Disruption of mitochondrial dynamics affects behaviour and lifespan in Caenorhabditis elegans. *Cell. Mol. Life Sci.* **76**: 1967–1985. [Medline] [CrossRef]
6. Conley, K. E., Amara, C. E., Jubrias, S. A. and Marcinek, D. J. 2007. Mitochondrial function, fibre types and ageing: new insights from human muscle *in vivo*. *Exp. Physiol.* **92**: 333–339. [Medline] [CrossRef]
7. Dahl, R., Larsen, S., Dohlmann, T. L., Qvortrup, K., Helge, J. W., Dela, F. and Prats, C. 2015. Three-dimensional reconstruction of the human skeletal muscle mitochondrial network as a tool to assess mitochondrial content and structural organization. *Acta Physiol. (Oxf.)* **213**: 145–155. [Medline] [CrossRef]
8. Hakamata, Y., Watanabe, K., Amo, T., Toyomizu, M. and Kikusato, M. 2018. Characterization of mitochondrial content and respiratory capacities of broiler chicken skeletal muscles with different muscle fiber compositions. *J. Poult. Sci.* **55**: 210–216. [Medline] [CrossRef]
9. Hosotani, M., Kawasaki, T., Hasegawa, Y., Wakasa, Y., Hoshino, M., Takahashi, N., Ueda, H., Takaya, T., Iwasaki, T. and Watanabe, T. 2020. Physiological and pathological mitochondrial clearance is related to pectoralis major muscle pathogenesis in broilers with wooden breast syndrome. *Front. Physiol.* **11**: 579. [Medline] [CrossRef]
10. Jarc, E. and Petan, T. 2019. Lipid droplets and the management of cellular stress. *Yale J. Biol. Med.* **92**: 435–452. [Medline]
11. Kawasaki, T., Yoshida, T. and Watanabe, T. 2016. Simple method for screening the affected birds with remarkably hardened pectoralis major muscles among broiler chickens. *J. Poult. Sci.* **53**: 291–297. [Medline] [CrossRef]
12. Kunz, W. S. 2001. Control of oxidative phosphorylation in skeletal muscle. *Biochim. Biophys. Acta* **1504**: 12–19. [Medline] [CrossRef]
13. Liesa, M., Palacín, M. and Zorzano, A. 2009. Mitochondrial dynamics in mammalian health and disease. *Physiol. Rev.* **89**: 799–845. [Medline] [CrossRef]

14. Listrat, A., Lebret, B., Louveau, I., Astruc, T., Bonnet, M., Lefaucheur, L., Picard, B. and Bugeon, J. 2016. How muscle structure and composition influence meat and flesh quality. *ScientificWorldJournal* **2016**: 3182746. [Medline] [CrossRef]
15. Liu, R., Jin, P., Yu, L., Wang, Y., Han, L., Shi, T. and Li, X. 2014. Impaired mitochondrial dynamics and bioenergetics in diabetic skeletal muscle. *PLoS One* **9**: e92810. [Medline] [CrossRef]
16. Malila, Y., Thanatsang, K., Arayamethakorn, S., Uengwetwanit, T., Srimarut, Y., Petracci, M., Strasburg, G. M., Rungrassamee, W. and Visessanguan, W. 2019. Absolute expressions of hypoxia-inducible factor-1 alpha (HIF1A) transcript and the associated genes in chicken skeletal muscle with white striping and wooden breast myopathies. *PLoS One* **14**: e0220904. [Medline] [CrossRef]
17. Nakamura, Y. N., Iwamoto, H., Shiba, N., Miyachi, H., Tabata, S. and Nishimura, S. 2004. Developmental states of the collagen content, distribution and architecture in the pectoralis, iliotibialis lateralis and puboischiofemoralis muscles of male Red Cornish x New Hampshire and normal broilers. *Br. Poult. Sci.* **45**: 31–40. [Medline] [CrossRef]
18. Papah, M. B., Brannick, E. M., Schmidt, C. J. and Abasht, B. 2017. Evidence and role of phlebitis and lipid infiltration in the onset and pathogenesis of Wooden Breast Disease in modern broiler chickens. *Avian Pathol.* **46**: 623–643. [Medline] [CrossRef]
19. Romanello, V. and Sandri, M. 2021. The connection between the dynamic remodeling of the mitochondrial network and the regulation of muscle mass. *Cell. Mol. Life Sci.* **78**: 1305–1328. [Medline] [CrossRef]
20. Sihvo, H. K., Immonen, K. and Puolanne, E. 2014. Myodegeneration with fibrosis and regeneration in the pectoralis major muscle of broilers. *Vet. Pathol.* **51**: 619–623. [Medline] [CrossRef]
21. Talbot, J. and Maves, L. 2016. Skeletal muscle fiber type: using insights from muscle developmental biology to dissect targets for susceptibility and resistance to muscle disease. *Wiley Interdiscip. Rev. Dev. Biol.* **5**: 518–534. [Medline] [CrossRef]
22. Tan, R., Nederveen, J. P., Gillen, J. B., Joanisse, S., Parise, G., Tarnopolsky, M. A. and Gibala, M. J. 2018. Skeletal muscle fiber-type-specific changes in markers of capillary and mitochondrial content after low-volume interval training in overweight women. *Physiol. Rep.* **6**: e13597. [Medline] [CrossRef]
23. Tarnopolsky, M. A., Rennie, C. D., Robertshaw, H. A., Fedak-Tarnopolsky, S. N., Devries, M. C. and Hamadeh, M. J. 2007. Influence of endurance exercise training and sex on intramyocellular lipid and mitochondrial ultrastructure, substrate use, and mitochondrial enzyme activity. *Am. J. Physiol. Regul. Integr. Comp. Physiol.* **292**: R1271–R1278. [Medline] [CrossRef]
24. Thai, T. Q., Nguyen, H. B., Saitoh, S., Wu, B., Saitoh, Y., Shimo, S., Elewa, Y. H. A., Ichii, O., Kon, Y., Takaki, T., Joh, K. and Ohno, N. 2016. Rapid specimen preparation to improve the throughput of electron microscopic volume imaging for three-dimensional analyses of subcellular ultrastructures with serial block-face scanning electron microscopy. *Med. Mol. Morphol.* **49**: 154–162. [Medline] [CrossRef]
25. Tilokani, L., Nagashima, S., Paupe, V. and Prudent, J. 2018. Mitochondrial dynamics: overview of molecular mechanisms. *Essays Biochem.* **62**: 341–360. [Medline] [CrossRef]
26. Vincent, A. E., Turnbull, D. M., Eisner, V., Hajnóczky, G. and Picard, M. 2017. Mitochondrial nanotunnels. *Trends Cell Biol.* **27**: 787–799. [Medline] [CrossRef]
27. Vincent, A. E., White, K., Davey, T., Philips, J., Ogden, R. T., Lawless, C., Warren, C., Hall, M. G., Ng, Y. S., Falkous, G., Holden, T., Deehan, D., Taylor, R. W., Turnbull, D. M. and Picard, M. 2019. Quantitative 3D mapping of the human skeletal muscle mitochondrial network. *Cell Rep.* **26**: 996–1009.e4. [Medline] [CrossRef]
28. Wang, Y. and Pessin, J. E. 2013. Mechanisms for fiber-type specificity of skeletal muscle atrophy. *Curr. Opin. Clin. Nutr. Metab. Care* **16**: 243–250. [Medline] [CrossRef]
29. Westermann, B. 2012. Bioenergetic role of mitochondrial fusion and fission. *Biochim. Biophys. Acta* **1817**: 1833–1838. [Medline] [CrossRef]
30. Youle, R. J. and van der Bliek, A. M. 2012. Mitochondrial fission, fusion, and stress. *Science* **337**: 1062–1065. [Medline] [CrossRef]
31. Zamponi, N., Zamponi, E., Cannas, S. A., Billoni, O. V., Helguera, P. R. and Chialvo, D. R. 2018. Mitochondrial network complexity emerges from fission/fusion dynamics. *Sci. Rep.* **8**: 363. [Medline] [CrossRef]